

The following resources related to this article are available online at www.sciencemag.org (this information is current as of October 8, 2007):

Updated information and services, including high-resolution figures, can be found in the online version of this article at:

<http://www.sciencemag.org/cgi/content/full/313/5783/87>

Supporting Online Material can be found at:

<http://www.sciencemag.org/cgi/content/full/313/5783/87/DC1>

This article **cites 16 articles**, 8 of which can be accessed for free:

<http://www.sciencemag.org/cgi/content/full/313/5783/87#otherarticles>

This article has been **cited by** 3 article(s) on the ISI Web of Science.

This article has been **cited by** 5 articles hosted by HighWire Press; see:

<http://www.sciencemag.org/cgi/content/full/313/5783/87#otherarticles>

This article appears in the following **subject collections**:

Geochemistry, Geophysics

http://www.sciencemag.org/cgi/collection/geochem_phys

Information about obtaining **reprints** of this article or about obtaining **permission to reproduce this article** in whole or in part can be found at:

<http://www.sciencemag.org/about/permissions.dtl>

Hydrogen Isotopes in Eocene River Gravels and Paleoelevation of the Sierra Nevada

Andreas Mulch,* Stephan A. Graham, C. Page Chamberlain

We determine paleoelevation of the Sierra Nevada, California, by tracking the effect of topography on precipitation, as recorded in hydrogen isotopes of kaolinite exposed in gold-bearing river deposits from the Eocene Yuba River. The data, compared with the modern isotopic composition of precipitation, show that about 40 to 50 million years ago the Sierra Nevada stood tall (≥ 2200 meters), a result in conflict with proposed young surface uplift by tectonic and climatic forcing but consistent with the Sierra Nevada representing the edge of a pre-Eocene continental plateau.

The evolution of mountainous topography reflects a balance between tectonic forces in Earth's lithosphere and upper mantle and erosion at Earth's surface. However, their relative roles remain controversial (1, 2). Understanding the long-term topographic history of the Sierra Nevada, California, figures importantly in this debate. One view is that the bulk of elevation gain took place in the Pliocene about 3 to 5 million years ago (Ma) (3–5) and is the result of removal of dense mantle lithosphere (6–8). In contrast, the Sierra Nevada may have existed as a major topographic feature throughout the Cenozoic (9–13) and the apparent young uplift may be due, in part, to climatic changes at 3 to 5 Ma (14, 15). To provide a further test, we determine Eocene (~40 to 50 Ma) stream gradients and headwater elevations by measuring the hydrogen isotope composition of kaolinite from Eocene fluvial sediments that record the isotopic composition of Eocene surface waters from ancient sea level continuously upstream into the modern (and ancient) range. One key piece of evidence cited for considerable (>1000 m) Pliocene surface uplift (5) comes from Eocene river gravels exposed along the western flank of the Sierra Nevada. These gravels, mined for gold in the later half of the 1800s, are nearly continuously exposed in open-cast mines from Eocene sea level upstream to current elevations of 2000 m, where they comprise the fill of bedrock-incised valleys and canyons, locally greater than 200 m deep. In this ancient fluvial system (16, 17), kaolinitized Eocene river deposits are overlain by Oligocene (38.9 Ma) volcanoclastic units, with the kaolinite formed during Eocene weathering of granitic fluvial detritus shortly after deposition in the ancestral Yuba River (18). Because kaolinite incorporates water into the crystal structure during its formation, its hydrogen isotopic composition (δD_{kaol}) serves as a

proxy for the isotopic composition of Eocene precipitation and near-surface ground water along the river channel. As in orogenic belts, the isotopic composition of precipitation scales with altitude, δD_{kaol} values are thus largely controlled by changes in elevation (19–22).

We determined 44 δD_{kaol} values (table S1) from 15 localities along the Eocene Yuba and American rivers (Fig. 1). We collected in situ kaolinite from individual granitic clasts, as well as samples from Eocene channel sands, which reflect detrital kaolinite transported from up-

stream. Both are from the upper part of the depositional sequence (commonly referred to as bench gravels) (fig. S2) (16, 17). The difference in δD_{kaol} from Eocene sea level to upstream weathering sites, $\Delta(\delta D_{\text{kaol}})$, provides an estimate of paleoelevation because the change in isotopic composition of precipitation, $\Delta(\delta D_{\text{ppt}})$, during ascent of cloud systems is related to the change in elevation (19, 20, 22). We convert $\Delta(\delta D_{\text{kaol}})$ to paleoelevation using a thermodynamic model (20) for isotopic lapse rates (fig. S1). This model includes Eocene sea surface temperature and relative humidity as inputs and reproduces equilibrium fractionation of $\delta^{18}\text{O}_{\text{ppt}}$ and δD_{ppt} between precipitation and water vapor, based on Rayleigh distillation of an air mass during orographic ascent (18). For elevations of 1000 to 2000 m, the modeled Eocene hydrogen isotope lapse rate ($-1.65\text{‰}/100$ m) and the measured modern lapse rate ($-1.70\text{‰}/100$ m) (23) are identical within error. The methodological error on the paleoelevation estimates is $\sim +350\text{--}400$ m (fig. S1).

For all three tributaries of the Eocene Yuba and adjacent American rivers, δD of in situ kaolinite decreases systematically upstream (Fig. 2) from $\delta D_{\text{kaol}} = -88\text{‰}$ at 400 m of modern elevation to $\delta D_{\text{kaol}} = -105\text{‰}$ at

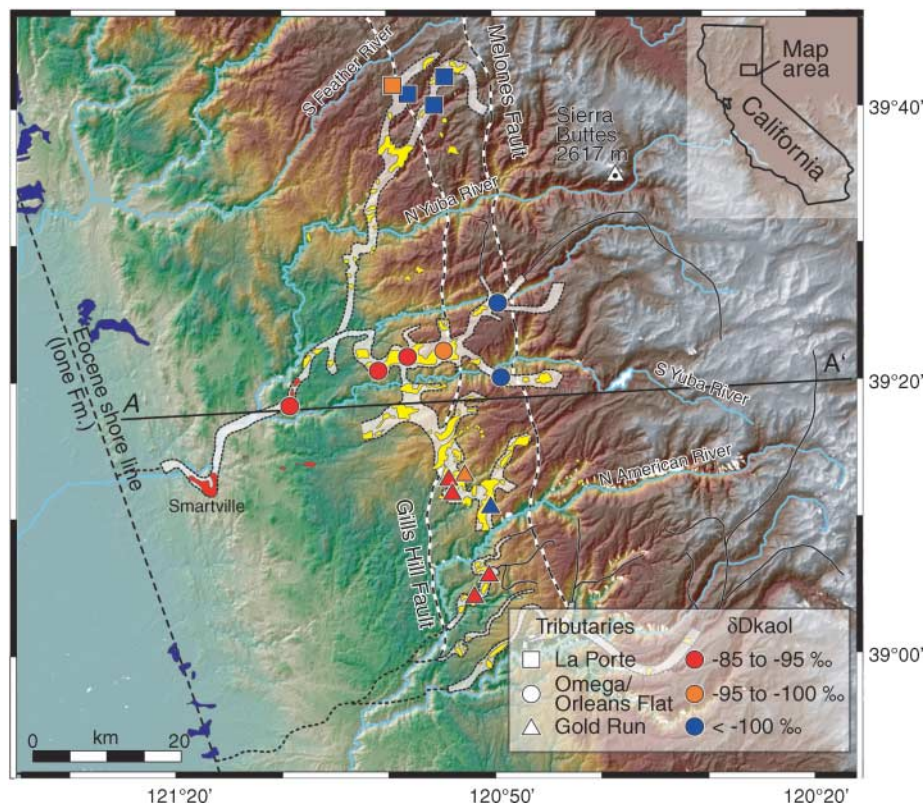


Fig. 1. Shaded relief map of northern Sierra Nevada. Sampling locations of kaolinitized river gravels shown by filled symbols and color-coded according to mean δD_{kaol} value. Eocene shoreline (9) is defined by coastal to marine lone Formation and temporally equivalent to deposition of gravels in the ancestral Yuba River. Reconstructed course of Eocene Yuba River (white) based on exposure of Eocene gravel (yellow). A-A' is profile in Fig. 3.

Geological and Environmental Sciences, Stanford University, 450 Serra Mall, Building 320, Stanford, CA 94305, USA.

*To whom correspondence should be addressed. E-mail: mulch@pangea.stanford.edu

~1600 m of modern elevation. In contrast, δD of detrital kaolinite is not correlated with distance from the Eocene shoreline but is identical to the most deuterium-depleted in situ kaolinite at the highest reaches of the Yuba River (Fig. 2). This result is expected, as detrital kaolinite should be transported downstream from its weathering location to the site of deposition. Systematic differences in δD of detrital and in situ kaolinite document that δD_{kaol} values reflect the conditions during Eocene weathering and that any postdepositional processes did not affect the δD_{kaol} in the river deposits (18).

Converting these isotopic compositions to paleoelevation requires knowledge of δD_{ppt} at a

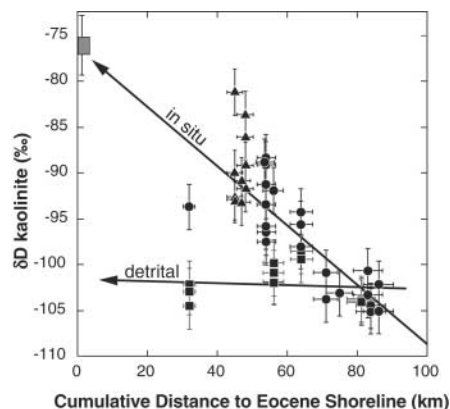
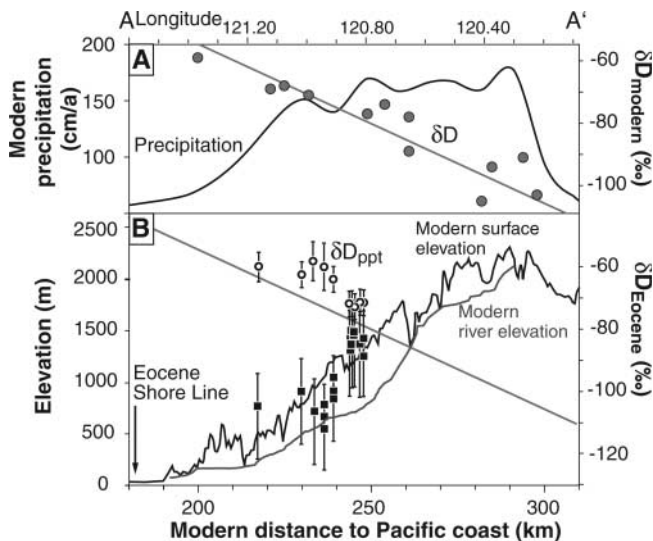


Fig. 2. δD_{kaol} along Eocene Yuba (circles) and American (triangles) rivers versus distance to Eocene shoreline. Linear regression through in situ δD_{kaol} from Yuba River indicates sea level $\delta D_{kaol} = -76 \pm 5\text{‰}$ ($r^2 = 0.76$) within error identical to kaolinite in isotopic equilibrium with modern precipitation at the Pacific coast (gray square). Detrital kaolinite (squares) overlaps with most D-depleted in situ kaolinite. The $25 \pm 5\text{‰}$ decrease in δD_{kaol} from sea level upstream reflects rainout during uplift of moisture along the western flank of the Eocene Sierra Nevada.

Fig. 3. (A) Orographic effect of northern Sierra Nevada as seen in amount and δD of precipitation along modern Yuba river (23, 27). Rainout across modern range correlates with strong decrease in δD_{ppt} . (B) A similar correlation between reconstructed Eocene elevation (squares) and calculated δD of Eocene local meteoric water (circles) is observed for the ancient Yuba River. Modern correlation from (A) shown for reference.



low elevation site. However, in situ kaolinite is not exposed in the lowest segments of the ancient Yuba River that we sampled, and the clay mineral inventory is dominated by detrital kaolinite. In the absence of isotopic data for kaolinite at Eocene sea level, we use a value based on a linear fit through δD_{kaol} (in situ) that gives a sea level intercept at $\delta D_{kaol} = -75 \pm 5\text{‰}$ ($r^2 = 0.76$) (Fig. 2). This value is lower than δD_{kaol} in equilibrium with precipitation recorded at most low-elevation, low-latitude ($<35^\circ$) stations in the modern International Atomic Energy Agency (IAEA) Global Network of Isotopes in Precipitation (18, 24). For the most conservative paleoelevation estimate we, therefore, adopt the lower bound on the sea level intercept ($\delta D_{kaol} = -80\text{‰}$) as our sea level δD_{kaol} , which results in lower estimated paleoelevations.

Based on the measured δD_{kaol} in the upstream regions of the La Porte, Omega, and Gold Run tributaries (Fig. 1), the average $\Delta(\delta D_{kaol})$ is -25‰ (Fig. 2). This value corresponds to an average Eocene elevation of the highest exposed ancestral Yuba River deposits of ~ 1.5 km (1503 +379/-498 m, including a 5% uncertainty on the δD_{kaol} at sea level) (Fig. 3) (18). Given that these deposits are found downstream of Eocene bedrock canyons, this elevation likely underestimates paleoelevation of the headwaters of the Eocene Yuba River, as low- δD waters must have flowed from adjacent mountaintops.

Three results come from our paleoaltimetry analysis. First, Eocene elevations for different tributaries of the ancestral Yuba River overlap within error with modern elevations. This result, seemingly at odds with paleoelevations inferred from studies based on differential tilt of Eocene and younger strata (3-5), suggests that the western slopes of the Eocene and the modern northern Sierra Nevada were similar.

Second, there is a larger scatter of calculated elevations observed at 40 to 60 km distance from the Eocene shoreline (Fig. 2). We suggest

that this scatter reflects the hypsometry of the drainage patterns along the northwest-trending aggradational segment of the ancient Yuba where the course of the river follows two major fault zones (Fig. 1). Within this northwest trending bedrock-controlled segment, we expect to see mixing of surface runoff from steep west-directed tributaries that drain high elevations to the east and meteoric water that reflects the local hypsometry along the more shallowly dipping range-parallel river segment.

Third, the result that reconstructed elevations for all three tributaries are identical suggests that they were draining a tall range with moderate relief. This is consistent with the measured Eocene bedrock incision that is commonly ~ 200 to 300 m but up to 790 m near the Sierra Buttes (4) (Fig. 1). Together with the 1503 +379/-498 m estimate for the elevation of the Eocene river bed, the bedrock incision data imply that Eocene elevations were 1.7 to 1.8 km in the northern Sierra Nevada and that peaks reached up to ~ 2200 m above sea level. Both the modern Yuba River headwaters (~ 2100 m) and peak elevations (~ 2780 m) in the northern Sierra Nevada are $\sim 25\%$ higher than in the Eocene, indicative of post-Eocene uplift of 350 to 600 m. This result is in agreement with estimates of 300 to 500 m of Pliocene (3 to 5 Ma) surface uplift of the Sierra Nevada as inferred from measured river incision rates (14). Because relative surface displacements between the western Basin and Range province and the northern Sierra Nevada are of Miocene and younger age (25), we speculate that the Eocene Sierra Nevada formed the western edge of a high-elevation landscape that characterized large areas of the western United

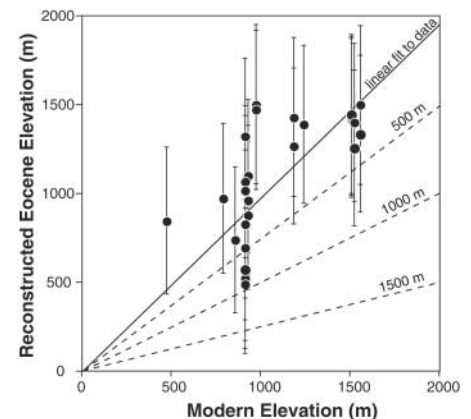


Fig. 4. Modern versus reconstructed Eocene sample elevations for ancestral Yuba River. Modern and Eocene elevations overlap within error, indicating that the Eocene Yuba River attained elevations similar to the interfluvies of the modern Yuba river where Eocene river deposits are preserved. Solid line is a fixed-sea level linear regression for the calculated Eocene elevations; dashed lines indicate expected trends for variable amounts of post-Eocene surface uplift.

States following Cretaceous thickening of the lithosphere (26). These stable isotope data alone do not preclude Pliocene surface uplift for the northern Sierra Nevada due to mantle delamination as has been proposed for the southern Sierra Nevada (6–8). In fact, our estimates of post-Eocene uplift are within the range of elevation change predictable for mantle delamination and may actually constrain the magnitude of mantle control on Pliocene surface uplift in the northern Sierra Nevada (Fig. 4). However, they are incompatible with a model of an Eocene low-elevation landscape that experienced substantial (1.5 to 2.0 km) Pliocene surface uplift. Calling upon a Pliocene age for major surface uplift in the northern Sierra Nevada would either require post-Eocene leveling of the mountains with subsequent renewed surface uplift or a tectonic and mechanical decoupling of the northern and southern Sierra Nevada, both of which are unrecognized in the geologic record.

References and Notes

1. P. Molnar, P. England, *Nature* **346**, 29 (1990).
2. C. Beaumont, R. A. Jamieson, M. H. Nguyen, B. Lee, *Nature* **414**, 738 (2001).
3. J. R. Unruh, *Geol. Soc. Am. Bull.* **103**, 1395 (1991).
4. J. Wakabayashi, T. L. Sawyer, *J. Geol.* **109**, 539 (2001).
5. C. H. Jones, G. L. Farmer, J. Unruh, *Geol. Soc. Am. Bull.* **116**, 1408 (2004).
6. G. Zandt et al., *Nature* **431**, 41 (2004).
7. M. N. Ducea, J. Saleeby, *Contrib. Mineral. Petrol.* **133**, 169 (1998).
8. J. Saleeby, M. N. Ducea, D. Clemens-Knott, *Tectonics* **22**, doi:10.1029/2002TC001374 (2003).
9. W. R. Dickinson, R. V. Ingersoll, S. A. Graham, *Geol. Soc. Am. Bull.* **90**, 1458 (1979).
10. B. Wernicke et al., *Science* **271**, 190 (1996).
11. M. A. House, B. P. Wernicke, K. A. Farley, *Nature* **396**, 66 (1998).
12. M. A. Poage, C. P. Chamberlain, *Tectonics* **21**, 1601 (2002).
13. M. K. Clark, G. Maheo, J. Saleeby, K. A. Farley, *GSA Today* **15**, 4 (2005).
14. G. M. Stock, R. S. Anderson, R. C. Finkel, *Earth Surf. Process. Landforms* **30**, 985 (2005).
15. E. E. Small, R. S. Anderson, *Science* **270**, 277 (1995).
16. W. Lindgren, *U.S. Geol. Surv. Prof. Pap.* **73** (1911).
17. W. H. Yeend, *U.S. Geol. Surv. Prof. Pap.* **722** (1974).
18. Available as supporting material on Science Online.
19. C. N. Garzione, J. Quade, P. G. DeCelles, N. B. English, *Earth Planet. Sci. Lett.* **183**, 215 (2000).
20. D. B. Rowley, R. T. Pierrehumbert, B. S. Currie, *Earth Planet. Sci. Lett.* **188**, 253 (2001).
21. A. Mulch, C. Teysier, M. A. Cosca, O. Vanderhaeghe, T. W. Vennemann, *Geology* **32**, 525 (2004).
22. M. A. Poage, C. P. Chamberlain, *Am. J. Sci.* **301**, 1 (2001).
23. N. L. Ingraham, B. E. Taylor, *Water Resources Res.* **27**, 77 (1991).
24. IAEA, <http://fishohis.iaea.org/userupdate/GNIP2001yearly.xls> (2001).
25. C. D. Henry, M. E. Perkins, *Geology* **29**, 719 (2001).
26. P. G. DeCelles, *Am. J. Sci.* **304**, 105 (2004).
27. Spatial Climate Analysis Service, Oregon State University, www.ocs.oregonstate.edu/prism, created April 2005.
28. We acknowledge C. H. Jones and two anonymous reviewers for thorough and constructive reviews. This work was supported by NSF grant EAR-0309011 to C.P.C.

Supporting Online Material

www.sciencemag.org/cgi/content/full/313/5783/87/DC1

Materials and Methods

Figs. S1 and S2

Table S1

References and Notes

8 February 2006; accepted 22 May 2006

10.1126/science.1125986

Antibiotic Stress Induces Genetic Transformability in the Human Pathogen *Streptococcus pneumoniae*

Marc Prudhomme,* Laetitia Attaiech,* Guillaume Sanchez, Bernard Martin, Jean-Pierre Claverys†

Natural transformation is a widespread mechanism for genetic exchange in bacteria. Aminoglycoside and fluoroquinolone antibiotics, as well as mitomycin C, a DNA-damaging agent, induced transformation in *Streptococcus pneumoniae*. This induction required an intact competence regulatory cascade. Furthermore, mitomycin C induction of *recA* was strictly dependent on the development of competence. In response to antibiotic stress, *S. pneumoniae*, which lacks an SOS-like system, exhibited genetic transformation. The design of antibiotherapy should take into consideration this potential of a major human pathogen to increase its rate of genetic exchange in response to antibiotics.

Bacterial transformation, originally discovered in the human pathogen *S. pneumoniae* (1), relies on a process that is inherent to the species, is independent of extrachromosomal elements, and can be considered the only programmed mechanism for generalized genetic exchange in bacteria. It allows the uptake and integration of exogenous DNA in the recipient genome and is considered to be a form of parasexuality (2). Transformation is believed to contribute to the genetic plasticity of *S. pneumoniae* and to play a central role in the adaptation of this pathogen to host defenses (3). We sought to establish whether transformation is induced in response to antibiotic stress.

Laboratoire de Microbiologie et Génétique Moléculaires, UMR 5100 CNRS-Université Paul Sabatier, 118 route de Narbonne, 31062 Toulouse Cedex 9, France.

*These authors contributed equally to this work.

†To whom correspondence should be addressed. E-mail: claverys@ibcg.bioutoul.fr

In *S. pneumoniae*, competence for genetic transformation is a transient physiological state allowing efficient DNA uptake (4) and a previously unrecognized capacity to kill non-competent cells (5, 6), a phenomenon referred to as pneumococcal fratricide (6) or sobrinicide (7). The development of competence requires transcriptional activation of the *com* regulon, which comprises 105 to 124 genes (8, 9), including *recA* (10). The RecA protein plays a key role in transformation by catalyzing homologous recombination between the internalized DNA and the recipient genome. The *com* regulon is induced when a competence-stimulating peptide (CSP), encoded by *comC* and exported through a dedicated secretion apparatus ComAB, accumulates in the medium and stimulates its receptor, the membrane-bound histidine kinase ComD (4). It is assumed that ComD then autophosphorylates and transphosphorylates its cognate response regulator ComE (11), which

in turn activates the expression of the so-called early *com* genes (4), including *comAB*, *comCDE*, and *comX*. The latter encodes an alternative sigma factor σ^X (12), which most probably recognizes a sequence (TACGAATA, hereafter called *Pcin*) conserved in the putative promoter regions of the late *com* genes (4, 9). The early control of competence induction is not yet fully understood. It was first suggested that competence induction relies simply on passive CSP accumulation, but we favor an alternative model in which CSP production could be temporarily increased in response to changes in environmental conditions (4, 13). We further propose that competence in *S. pneumoniae* is a general stress response, playing a role similar to that of the SOS response in *Escherichia coli* (4).

We tested this hypothesis by investigating the effect of mitomycin C, a DNA-damaging agent known to induce the SOS response, on the *com* regulon. To monitor competence induction (14), we used transcriptional fusions with the *luc* gene from the firefly (*Photinus pyralis*) encoding luciferase, the activity of which can be monitored directly in living *S. pneumoniae* cells (14). We first used a fusion of *luc* with *ssbB*, a representative of the late *com* genes (8, 9), which encodes a single-stranded DNA-binding protein (15). Luciferase activity was monitored during growth with various concentrations of mitomycin C. Expression of the reporter was stimulated by exposure to 25 to 60 ng ml⁻¹ of mitomycin C (Fig. 1A and fig. S1A), indicating that *ssbB* was induced when cells were grown in the presence of the DNA-damaging agent. No induction of the same fusion was detected in a *comA* mutant background [that is, in a strain unable to export CSP and therefore to develop spontaneous competence (Fig. 1B)], demonstrating that an